PHYSICAL REVIEW B **96**, 201112(R) (2017)

Time-reversal-symmetric topological magnetoelectric effect in three-dimensional topological insulators

Heinrich-Gregor Zirnstein and Bernd Rosenow
Institut für Theoretische Physik, Universität Leipzig, D-04103 Leipzig, Germany
(Received 12 May 2017; revised manuscript received 27 September 2017; published 27 November 2017)

One of the hallmarks of time-reversal-symmetric topological insulators in three dimensions is the topological magnetoelectric effect (TME). So far, a time-reversal breaking variant of this effect has attracted much attention, in the sense that the induced electric charge changes sign when the direction of an externally applied magnetic field is reversed. Theoretically, this effect is described by the so-called axion term. Here, we discuss a time-reversal-symmetric TME, where the electric charge depends only on the magnitude of the magnetic field but is independent of its sign. We obtain this nonperturbative result both analytically and numerically, and suggest a mesoscopic setup to demonstrate it experimentally.

DOI: 10.1103/PhysRevB.96.201112

Introduction. Time-reversal-symmetric (TRS) topological insulators (TIs) [1,2] are a fascinating class of electronic materials with insulating bulk and topologically protected surface states, which are either gapless, break a symmetry, or feature topological order [3]. Evidence for the existence of such surface states comes from spin textures observed in photoemission experiments [4,5] and from the observation of a half-integer quantum Hall effect [6–9].

From a theoretical point of view, the hallmark response of TRS TIs in three dimensions (3D) is the topological magnetoelectric effect [10,11]. So far, a time-reversal (TR) breaking variant of this effect has attracted much attention. When TR is broken by, say, a magnetic coating with Zeeman coupling to the TI surface, a Hall conductivity $\sigma_{xy} = \frac{\tilde{\theta}}{2\pi}\frac{e^2}{2\pi}$ arises, where $\tilde{\theta}$ is quantized to $\tilde{\theta} = \pm\pi$. Then, the insertion of a magnetic flux tube gives rise to the accumulation of a charge $|Q| = e/2$ per flux quantum $\Phi_0 = h/e$. Importantly, $\mathrm{sgn}(Q)$ depends on the direction of the magnetic field inside the flux tube, i.e., the response is not TRS. A consequence of the surface Hall conductivity is quantized Kerr and Faraday rotations [12,13], which have recently been confirmed experimentally [14–16].

In the presence of TRS, the linear magnetoelectric response vanishes [17,18]. Thus, strictly speaking, all variants of the topological magnetoelectric effect are nonlinear effects, as they require an additional perturbation, say, a Zeeman coupling on the surface as above. The absence of a linear magnetoelectric response may seem to be at odds with the fact that the bulk of a 3D TRS TI has been characterized by the so-called axion action [10,11] $S_\theta = \frac{\theta}{2\pi}\frac{e^2}{2\pi}\int d^3x\, dt\, \mathbf{E}\cdot\mathbf{B}$. Under a TR transformation, $\mathbf{E} \to \mathbf{E}$, $\mathbf{B} \to -\mathbf{B}$, and $S_\theta \to -S_\theta$. Classically, this action breaks TRS, but quantum mechanically, only the Feynman amplitude e^{iS_θ} needs to be symmetric. If the electronic wave functions and electromagnetic fields satisfy periodic boundary conditions, one can show that this integral is quantized to integer multiples of $4\pi^2/e^2$ [19,20]. This implies that $S_\theta = \theta$ modulo 2π, hence $\theta = \pm\pi$ would respect TRS also. Now, for a TI with boundaries, by using partial integration, $S_{\pm\pi}$ can be converted into the surface quantum Hall term discussed above, and it seems naively that the axion action indeed describes a magnetoelectric effect. However, this is not the case, as the surface response due to $S_{\pm\pi}$ is canceled by additional contributions from the surface states, in this case the parity anomaly, to restore TRS [21–23].

In this work, we describe a TR-symmetric topological magnetoelectric effect. This means that the accumulated electric charge depends only on the magnitude of the magnetic flux but is independent of its sign (magnetic field direction). In particular, we consider a spherical TI threaded by a thin magnetic flux tube, and subject to a small uniform electric field [see Fig. 1(a)]. If $Q_{\mathrm{top}}(\mathbf{E}_z,\Phi)$ denotes the total charge on the top half, we show that the additional charge due to the insertion of one flux quantum is $\Delta Q(\mathbf{E}_z,\pm\Phi_0) \equiv Q_{\mathrm{top}}(\mathbf{E}_z,\pm\Phi_0) - Q_{\mathrm{top}}(\mathbf{E}_z,0) = +(e/2)\,\mathrm{sgn}\,\mathbf{E}_z$. This response is TRS, in contrast to the TR-breaking surface quantum Hall effect [6–9,24–28] described above. In addition, we numerically analyze a lattice model, and suggest a mesoscopic setup to demonstrate this effect experimentally. These results are not related to the wormhole effect [29], which only occurs when the diameter of the flux tube is much smaller than the lattice spacing. Here, we instead consider a flux tube that covers many plaquettes, so that the surface states of the TI can be described by a continuum two-dimensional (2D) Dirac Hamiltonian. Then, on an infinite planar surface, inserting one flux quantum Φ_0 will give rise to a single, spin-polarized zero-energy state localized (power law) at the tube [30–32]. Our treatment of a finite geometry goes significantly beyond this result.

Physical picture. The fractional charge $e/2$ arises because an occupied delocalized eigenstate is transformed into an occupied localized eigenstate when adiabatically inserting one flux quantum: In a spherical geometry, the delocalized state has equal weight in both hemispheres, whereas the localized state is contained in one of them; this corresponds to a change of charge in that hemisphere by $e/2$. The presence of a small background field $\mathbf{E}_z$ is important for this to happen: Flux insertion generates two localized states, one at each pole, which would otherwise hybridize with each other, resulting in delocalized eigenstates again, and no charge difference would be observable. Only when the energy difference between the localized states, due to $\mathbf{E}_z$, is larger than the hybridization, one localized state will be occupied, and the other one empty.

In order to evaluate the induced charge, we compute the two eigenstates with energies closest to the Fermi level for each value of the flux Φ between zero and Φ_0, and then evaluate the effect of an external electric field $\mathbf{E}_z$ in the subspace spanned by these states. This projection to a low-energy subspace becomes

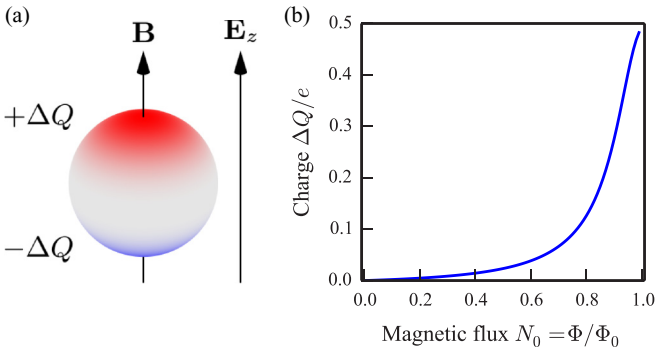

FIG. 1. Spherical topological insulator threaded by a thin magnetic flux tube with flux Φ and subject to an electric field $\mathbf{E}_z$ in vertical direction. Insertion of one flux quantum induces a charge $\Delta Q = e/2$. (a) Geometry. (b) Analytical result for the charge difference in the top hemisphere, $\Delta Q(\mathbf{E}_z, \Phi)$, in the thin flux tube limit for an external electric field $\mathbf{E}_z$, giving rise to a potential energy difference $e2RE_z$ between top and bottom, with $e2RE_z = 0.2v_F/R$. Here, R denotes the radius of the sphere and v_F is the Fermi velocity on the surface.

exact if one first takes the limit of an infinitesimally thin flux tube [see Fig. 2(a)], and then considers an infinitesimal electric field $\mathbf{E}_z$. In this way, the infinitesimal $\mathbf{E}_z$ does not polarize the system for zero flux, but due to the order of limits described above, at $\Phi = \Phi_0$ the level splitting caused by $\mathbf{E}_z$ is much larger that the hybridization energy. In a numerical calculation, both the flux tube diameter and the electric field are small but finite, and the exact analytic result is recovered by finite-size scaling [see Fig. 3(b)].

The two lowest-energy eigenstates are superpositions of spin-polarized wave functions $\eta_n(\Phi,\mathbf{x})$ and $\eta_s(\Phi,\mathbf{x})$ located at the north and south pole; explicit expressions are derived later. Projecting to these states, the Hamiltonian becomes $\hat{H} = \Delta s_x + V s_z$ where s_x, s_z are Pauli matrices, Δ is the hybridization energy, and V is the projected potential energy

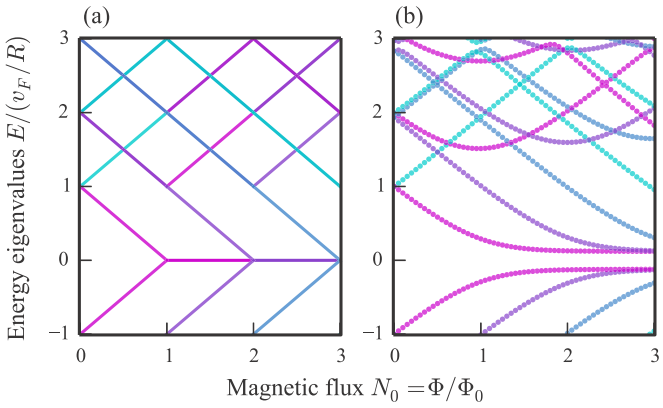

FIG. 2. Low-energy spectrum of a TI with a magnetic flux tube. (a) Analytical results for a spherical geometry in the limit of a thin flux tube. Angular momentum $m = \pm\frac{1}{2}, \pm\frac{3}{2}, \ldots$ is encoded by different colors. (b) Numerical results for the lattice model, Eq. (11), in a cuboid geometry with $10 \times 10 \times 8$ sites, a flux tube spanning 3×3 plaquettes, and parameters $\lambda = 1$, $t = 2$, and $\kappa = 4t$. The hybridization of the low-energy states after one flux quantum is due to the finite size of the flux tube.

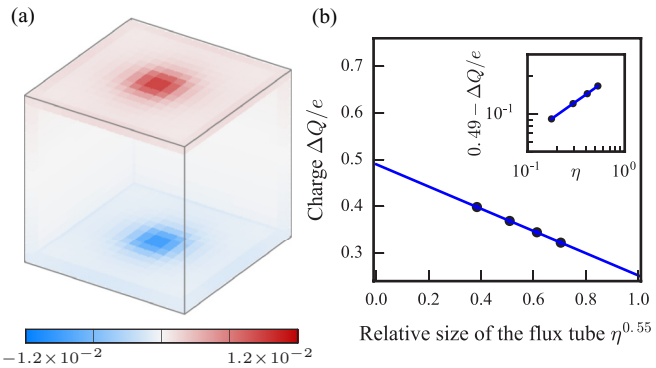

FIG. 3. Charge induced in the TI lattice model, Eq. (11), in a cuboid geometry with $18 \times 18 \times 18$ sites in the presence of a magnetic flux tube of unit flux $\Phi/\Phi_0 = 1$. Parameters are $\lambda = 2.43$, $t = \lambda$, $\kappa = 4t$, and $eU = 0.3\lambda$. (a) Charge distribution for a flux tube spanning 5×5 plaquettes. (b) Scaling of the total induced charge in the top half of the cube depending on the relative size η of the flux tube ($\eta \propto$ tube diameter). The inset shows that the charge scales according to a power law.

$V(\Phi) = ed(\Phi)\mathbf{E}_z$ with $d(\Phi) = \langle \eta_n | \mathbf{x}_3 | \eta_n \rangle$ the dipole moment. The charge response is $\Delta Q(\mathbf{E}_z, \Phi) = \rho(\mathbf{E}_z, \Phi) - \rho(\mathbf{E}_z, 0)$ with

$$\rho(\mathbf{E}_z, \Phi) = \frac{e}{2} \frac{w(\Phi)}{\sqrt{V(\Phi)^2 + \Delta(\Phi)^2}} V(\Phi), \tag{1}$$

and $w(\Phi) = \int_{\text{top}} d\mathbf{x}\, [|\eta_n(\Phi,\mathbf{x})|^2 - |\eta_s(\Phi,\mathbf{x})|^2]$. In the limit of a thin flux tube, the hybridization equals the energy $\Delta(\Phi) = (\Phi/\Phi_0 - 1)v_F/R$ for $\Phi < \Phi_0$ where v_F is the Fermi velocity and R the radius of the sphere. The corresponding charge response is depicted in Fig. 1(b). Since we have $\Delta(\Phi) \to 0$ and $w(\Phi) \to 1$ for $\Phi \to \Phi_0$, an infinitesimally small electric field is sufficient to lift the degeneracy, and we find that $\Delta Q(\mathbf{E}_z, \Phi_0) = +(e/2)\,\text{sgn}\,\mathbf{E}_z$ for $\mathbf{E}_z \to 0$.

Fractional charge. The appearance of a half-integer charge due to localized zero-energy states can be interpreted as an instance of charge fractionalization [31,33–35]. To make the connection to condensed matter, we consider a general lattice Hamiltonian $\hat{H}(A_0, \mathbf{A})$ which depends on an electric potential A_0 and a vector potential $\mathbf{A}$, and has n internal degrees of freedom per site $\mathbf{x}$. At zero temperature and chemical potential, the expectation value of the charge density is

$$\langle \hat{\rho}(\mathbf{x}) \rangle_{A_0,\mathbf{A}} = (-e) \sum_{E_\alpha \leqslant 0} |\eta_\alpha(\mathbf{x})|^2, \tag{2}$$

where E_α are the energy eigenvalues of $\hat{H}(A_0, \mathbf{A})$, and $\eta_\alpha(\mathbf{x})$ the corresponding eigenfunctions. We now focus on Hamiltonians with a chiral pseudosymmetry, described by a local operator $\hat{C}$ anticommuting with the Hamiltonian at zero electric field, $\{\hat{H}(A_0 = 0, \mathbf{A}), \hat{C}\} = 0$. Microscopically, such a pseudosymmetry can be realized for Hamiltonians defined on a bipartite lattice, with hoppings only between sublattices. Anticommutation implies that eigenstates come in pairs with positive and negative energy $E = E_\alpha = -E_\beta$, and locality means that the corresponding eigenfunctions have equal probabilities, $|\eta_\beta(\mathbf{x})|^2 = |\hat{C}\eta_\alpha(\mathbf{x})|^2 = |\eta_\alpha(\mathbf{x})|^2$. In particular, each probability can be expressed as half the sum of a positive and a negative energy eigenstate, $|\eta_\alpha(\mathbf{x})|^2 =$

$\frac{1}{2}(|\eta_\alpha(\mathbf{x})|^2 + |\eta_\beta(\mathbf{x})|^2)$. In the absence of zero-energy states, whose consequences will be discussed shortly, $E_\alpha \neq 0$, we can apply the above decomposition to Eq. (2), and find that the charge density can be expressed as $1/2$ times the sum over all eigenstates. But this sum corresponds to all bands completely filled, hence the electron density in the absence of an electric field is *spatially uniform* and has the constant value $\langle\hat{\rho}(\mathbf{x})\rangle_{A_0=0,\mathbf{A}} = (-e)n/2$.

The charge deviation from a reference configuration without fields is $\delta\langle\hat{\rho}(\mathbf{x})\rangle_{A_0,\mathbf{A}} = \langle\hat{\rho}(\mathbf{x})\rangle_{A_0,\mathbf{A}} - \langle\hat{\rho}(\mathbf{x})\rangle_{A_0=0,\mathbf{A}=0}$. Being constant, the reference charge density is $1/2$ times the sum over any complete set of states, giving

$$\delta\langle\hat{\rho}(\mathbf{x})\rangle_{A_0,\mathbf{A}} = (-e)\left[\frac{1}{2}\sum_{E_\alpha\leqslant 0}|\eta_\alpha(\mathbf{x})|^2 - \frac{1}{2}\sum_{E_\beta>0}|\eta_\beta(\mathbf{x})|^2\right]. \tag{3}$$

In high-energy physics, this expression defines the vacuum charge [31,33]. Here, an occupied state contributes a total charge of $\delta Q = -e/2$, an empty state contributes $\delta Q = +e/2$, while zero-energy states are ambiguous and can be attributed to either sum. In our setup, the magnetic flux gives localized zero-energy states, and this formula now describes a physical, localized charge deviation $\delta Q = \mp e/2$ whose sign is determined by the occupation of the states selected by the infinitesimal electric field $\mathbf{E}_z$.

Analytical results. Since the low-energy states of a TI are localized on the surface [18], we consider the Dirac Hamiltonian on a sphere with radius R [26,36,37],

$$\hat{H} = \begin{pmatrix} 0 & h^+ \\ h^- & 0 \end{pmatrix},$$
$$h^\pm = \mp\left(\partial_\theta + \frac{1}{2}\cot\theta\right) + \frac{i\partial_\phi}{\sin\theta} + eR\mathbf{A}_\phi, \tag{4}$$

where $\phi \in [0,2\pi)$, $\theta \in [0,\pi]$ are spherical coordinates, and energy is measured in units of v_F/R with v_F denoting the velocity of Dirac electrons. We have specialized to a vector potential $\mathbf{A}$ which has only an azimuthal component $\mathbf{A}_\phi(\theta)$, reflecting rotational symmetry around the flux tube. We can decompose $\psi(\phi,\theta) = \tilde{\psi}(\theta)e^{im\phi}/\sqrt{R}$ with half-integer angular momentum $m = \pm\frac{1}{2},\pm\frac{3}{2},\ldots$ for spin-1/2 electrons. In the absence of an external field, $\mathbf{A}_\phi = 0$, the energy eigenvalues of the spherical Dirac operator are known to be nonzero integers $E = \pm1,\pm2,\ldots$ whose multiplicities increase with angular momentum [38,39]. It is tempting to incorporate the flux tube by using the Aharonov-Bohm effect and shifting the angular momentum, $m \to m - N_0$ [26], where $N_0 = \Phi/\Phi_0$ is the number of flux quanta, but this approach does not allow the implementation of the correct boundary condition that the wave function $\tilde{\psi}(\theta)$ stays finite as $\theta \to 0,\pi$ for spatial coordinates *within the region of the flux tube* [40].

To model the flux tube, we express the vector potential as $N_\phi(\theta) = eR\mathbf{A}_\phi(\theta)\sin\theta$ and substitute $x = \cos\theta$. Then, we choose $N_\phi(x) = N_0\min\{1,(1-|x|)/\delta\}$, which is equal to the total flux N_0 in most of the sphere, but vanishes at the poles. For a thin flux tube, we have $0 < \delta \ll 1$. Using that $\hat{H}^2 = \mathrm{diag}(h^+h^-,h^-h^+)$, we only need to solve the eigenvalue equation $h^+h^-\psi_\uparrow = E^2\psi_\uparrow$. Then, the eigenvectors of the original Hamiltonian are obtained as $\psi_{\pm E} = (\pm E\psi_\uparrow, h^-\psi_\uparrow)^T$ if $E \neq 0$. Zero modes, $E = 0$, are obtained from $h^-\psi_\uparrow = 0$, or $h^+\psi_\downarrow = 0$. One finds that

$$h^+h^- = -\frac{d}{dx}\left[(1-x^2)\frac{d}{dx}\right] + \frac{1}{1-x^2}\left[-m + \frac{1}{2}x + N_\phi\right]^2 + \frac{dN_\phi}{dx} + \frac{1}{2}, \tag{5}$$

resembling the Legendre differential operator. This is a special case of the Schrödinger-Lichnerowicz formula [41]. We now use a piecewise ansatz [36,39], here shown for angular momentum $m \geqslant 1/2$:

$$\psi_\uparrow(x) = \begin{cases} (1-x)^{(1/2)(m-1/2)}(1+x)^{(1/2)(m+1/2)-(N_0/\delta)}g_0(x) \\ (1-x)^{(1/2)(m-N_0-1/2)}(1+x)^{(1/2)(m-N_0+1/2)}g(x) \\ (1-x)^{(1/2)(m-1/2)-(N_0/\delta)}(1+x)^{(1/2)(m+1/2)}g_1(x), \end{cases} \tag{6}$$

where the pieces are defined for $1-\delta \leqslant x \leqslant 1$, $|x| < 1-\delta$, and $-1 \leqslant x \leqslant -1+\delta$, respectively. We emphasize that the wave function stays finite near the poles. In coordinates $\xi = (1-x)/2$, the eigenvalue equation is equivalent to a set of hypergeometric equations for the functions $g_0(\xi),g(\xi),g_1(\xi)$, solved by hypergeometric functions $F(a,b,c;\xi)$ [42]. Abbreviating $c = (m+1/2-N_0)$ and assuming $c \notin \mathbb{Z}$, the general solution for the middle part is

$$g(\xi) = \alpha F(c-E,c+E,c,\xi) + \beta\xi^{1-c}F(1-E,1+E,2-c,\xi) \tag{7}$$

with parameters α,β that have to be determined by two jump conditions for derivatives, the first one being

$$g'(\varepsilon)/g(\varepsilon) - g_0'(\varepsilon)/g_0(\varepsilon) = N_0/\varepsilon \tag{8}$$

with $\varepsilon = \delta/2$, and the other similar [18]. To make progress, we now take the limit of a thin flux tube, $\varepsilon \to 0$. Expanding the solutions g_0,g_1 to leading order in ε while ignoring powers of order $\varepsilon^{|c|}$ or higher, we find [18] that the jump conditions can only be satisfied for energies E that fulfill

$$E = \pm\begin{cases} c+n & \text{if } c > 0 \\ 0 \text{ or } 1-c+n & \text{if } c < 0, \end{cases} \tag{9}$$

where $n = 0,1,2,\ldots$. This spectrum is visualized in Fig. 2(a).

We can now give explicit wave functions for the two eigenstates with energy closest to zero, used in Eq. (1). For flux $0 < \Phi < \Phi_0$, they have angular momentum $m = 1/2$ and are superpositions $\eta_\mp = (\eta_\mathrm{n} \pm \eta_\mathrm{s})/\sqrt{2}$ of states $\eta_\mathrm{n}(\mathbf{x}) = [\psi_\uparrow(x),0]^T$ and $\eta_\mathrm{s}(\mathbf{x}) = [0,\psi_\uparrow(-x)]^T$ with

$$\psi_\uparrow(x) = \frac{1}{\sqrt{\mathcal{N}}}(1-x)^{(1/2)(-\Phi/\Phi_0)}(1+x)^{(1/2)(1-\Phi/\Phi_0)} \tag{10}$$

in the region $|x| < 1-\delta$ and with normalization $\mathcal{N} = R[\sqrt{\pi}\Gamma(c)/\Gamma(c+1/2) + O(\delta^c)]$.

Numerical results. To confirm our analytic result, we have performed a numerical calculation using a minimal lattice model for a topological insulator [10]. This model concerns a four-component fermionic wave function on a cubic lattice. In

momentum (Bloch) space, the TR-symmetric Hamiltonian is

$$\hat{H} = -2\lambda\tau_z \sum_{\mu=1}^{3} \sigma_\mu \sin(k_\mu) + \tau_x \left(\kappa - 2t \sum_{\mu=1}^{3} \cos(k_\mu) \right), \tag{11}$$

where λ,κ,t are real parameters, and σ_μ and τ_μ are Pauli matrices acting on the spin (respectively, orbital) degrees of freedom. This model is a (strong) topological insulator in the parameter range $2t \leqslant \kappa \leqslant 6t$ [10]. Coupling to the electromagnetic field is achieved by Peierls substitution [18].

The induced charge in the presence of a flux tube and a small electric field is shown in Fig. 3. The charge distribution $\delta\langle\hat{\rho}(\mathbf{x})\rangle_{A_0,\mathbf{A}}$ is TR symmetric, localized on the surface, and concentrated at the flux tube. To compare with the analytical results, we need to take the limit of a thin flux tube by a scaling analysis where we fix a system size and shrink the size of the flux tube. The electric potential has to be smaller than the level spacing, but larger than the hybridization, as the order of limits is important. We find that the extrapolated value of the charge difference in the top half is $\Delta Q(\Phi_0) = +(0.49 \pm 0.02)e$, in excellent agreement with our analytical results. For a topologically trivial insulator (e.g., $6t < \epsilon$, not shown) no significant charge is accumulated at the flux tube.

Experimental realization. A mesoscopic setup for measuring the TR-symmetric charge response is illustrated in Fig. 4. If we use Bi_2Se_3 as an example TI [4] with a Fermi velocity $v_F \sim 5 \times 10^5$ m s^{-1} and assume that the system has a diameter of 1 μm, then the level spacing (9) of the surface states, $\Delta E = \hbar v_F/R$, should be on the order of half a meV. This is well below the bulk band gap $E_{\text{gap}} \sim 0.35$ eV, but large enough to be comparable to an externally applied voltage. A thin magnetic flux tube could be generated by using a superconductor to focus the magnetic field, or by pinning two magnetic vortices, or a giant vortex [44,45]. The numerical results, Fig. 3, indicate that larger tube diameters still yield an appreciable charge response, and the value for a thin tube can be obtained by finite-size scaling. The key signature of a TI is that the charge is a half-integer multiple of the elementary charge, as opposed to an integer multiple for purely 2D materials like graphene. Such an experiment is expected to be challenging but within reach of present day technology.

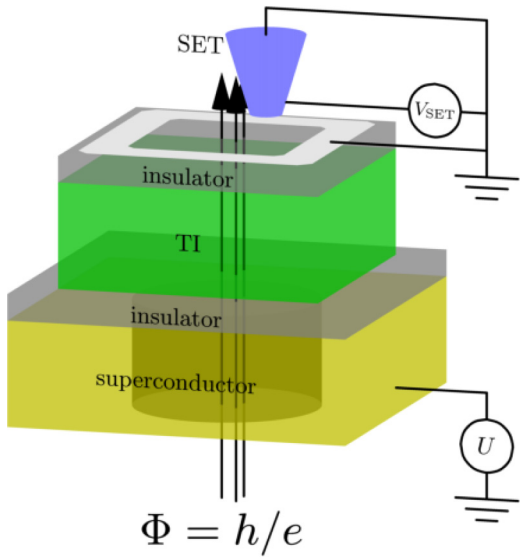

FIG. 4. Illustration of an experimental setup to measure the TRS surface charge. A superconductor focuses the magnetic flux through the TI, while a scanning single-electron transistor (SET) allows sensitive charge measurements [43]. The top and bottom sides of the TI have a voltage difference U.

Conclusion. While the electromagnetism of TRS TIs in 3D is commonly associated with the axion action, we have argued that this action is inadequate for describing a physical response, in particular one that is TRS. In search of the latter, we have adapted the idea of charge fractionalization from high-energy physics to a condensed-matter setting. Our main result is that the insertion of a thin flux tube leads to a pair of localized states whose hybridization at one flux quantum is much smaller than the level spacing. Combined with small background electric field, this allows us to adiabatically transform a delocalized eigenstate into a localized eigenstate, giving a TRS charge response of $e/2$ that is, in principle, amenable to experimental detection.

Acknowledgments. We would like to thank J. Smet and L. Kimme for helpful discussions. This publication was funded by the German Research Foundation within the Collaborative Research Centre 762 (project B6).

[1] M. Z. Hasan and C. L. Kane, Rev. Mod. Phys. **82**, 3045 (2010).
[2] X.-L. Qi and S.-C. Zhang, Rev. Mod. Phys. **83**, 1057 (2011).
[3] A. Vishwanath and T. Senthil, Phys. Rev. X **3**, 011016 (2013).
[4] Y. Xia, D. Qian, D. Hsieh, L. Wray, A. Pal, H. Lin, A. Bansil, D. Grauer, Y. S. Hor, R. J. Cava, and M. Z. Hasan, Nat. Phys. **5**, 398 (2009).
[5] H. Zhang, C.-X. Liu, X.-L. Qi, X. Dai, Z. Fang, and S.-C. Zhang, Nat. Phys. **5**, 438 (2009).
[6] C. Brüne, C. X. Liu, E. G. Novik, E. M. Hankiewicz, H. Buhmann, Y. L. Chen, X. L. Qi, Z. X. Shen, S. C. Zhang, and L. W. Molenkamp, Phys. Rev. Lett. **106**, 126803 (2011).
[7] C.-Z. Chang, J. Zhang, X. Feng, J. Shen, Z. Zhang, M. Guo, K. Li, Y. Ou, P. Wei, L.-L. Wang, Z.-Q. Ji, Y. Feng, S. Ji, X. Chen, J. Jia, X. Dai, Z. Fang, S.-C. Zhang, K. He, Y. Wang, L. Lu, X.-C. Ma, and Q.-K. Xue, Science **340**, 167 (2013).
[8] Y. Xu, I. Miotkowski, C. Liu, J. Tian, H. Nam, N. Alidoust, J. Hu, C.-K. Shih, M. Z. Hasan, and Y. P. Chen, Nat. Phys. **10**, 956 (2014).
[9] R. Yoshimi, A. Tsukazaki, Y. Kozuka, J. Falson, K. S. Takahashi, J. G. Checkelsky, N. Nagaosa, M. Kawasaki, and Y. Tokura, Nat. Commun. **6**, 6627 (2015).
[10] X.-L. Qi, T. L. Hughes, and S.-C. Zhang, Phys. Rev. B **78**, 195424 (2008).
[11] A. M. Essin, A. M. Turner, J. E. Moore, and D. Vanderbilt, Phys. Rev. B **81**, 205104 (2010).
[12] W.-K. Tse and A. H. MacDonald, Phys. Rev. Lett. **105**, 057401 (2010).
[13] J. Maciejko, X.-L. Qi, H. D. Drew, and S.-C. Zhang, Phys. Rev. Lett. **105**, 166803 (2010).

[14] L. Wu, M. Salehi, N. Koirala, J. Moon, S. Oh, and N. P. Armitage, Science **354**, 1124 (2016).
[15] K. N. Okada, Y. Takahashi, M. Mogi, R. Yoshimi, A. Tsukazaki, K. S. Takahashi, N. Ogawa, M. Kawasaki, and Y. Tokura, Nat. Commun. **7**, 12245 (2016).
[16] V. Dziom, A. Shuvaev, A. Pimenov, G. V. Astakhov, C. Ames, K. Bendias, J. Böttcher, G. Tkachov, E. M. Hankiewicz, C. Brüne, H. Buhmann, and L. W. Molenkamp, Nat. Commun. **8**, 15197 (2017).
[17] L. D. Landau and E. M. Lifschitz, *Electrodynamics of Continuous Media*, 2nd ed., Vol. 8 (Pergamon, New York, 1984).
[18] See Supplemental Material at http://link.aps.org/supplemental/10.1103/PhysRevB.96.201112 for details regarding time-reversal symmetry and the calculation of the eigenstates in the presence of a thin magnetic flux tube.
[19] J. W. Milnor and J. D. Stasheff, *Characteristic Classes* (Princeton University Press, Princeton, NJ, 1974).
[20] M. M. Vazifeh and M. Franz, Phys. Rev. B **82**, 233103 (2010).
[21] M. Mulligan and F. J. Burnell, Phys. Rev. B **88**, 085104 (2013).
[22] H.-G. Zirnstein and B. Rosenow, Phys. Rev. B **88**, 085105 (2013).
[23] E. Witten, Rev. Mod. Phys. **88**, 035001 (2016).
[24] K. Nomura and N. Nagaosa, Phys. Rev. Lett. **106**, 166802 (2011).
[25] E. J. König, P. M. Ostrovsky, I. V. Protopopov, I. V. Gornyi, I. S. Burmistrov, and A. D. Mirlin, Phys. Rev. B **90**, 165435 (2014).
[26] D.-H. Lee, Phys. Rev. Lett. **103**, 196804 (2009).
[27] O. Vafek, Phys. Rev. B **84**, 245417 (2011).
[28] F. S. Nogueira, Z. Nussinov, and J. van den Brink, Phys. Rev. Lett. **117**, 167002 (2016).
[29] G. Rosenberg, H. M. Guo, and M. Franz, Phys. Rev. B **82**, 041104 (2010).
[30] Y. Aharonov and A. Casher, Phys. Rev. A **19**, 2461 (1979).
[31] R. Jackiw and J. R. Schrieffer, Nucl. Phys. B **190**, 253 (1981).
[32] A. P. Polychronakos, Nucl. Phys. B **283**, 268 (1987).
[33] I. V. Krive and A. S. Rozhavskiĭ, Sov. Phys. Usp. **30**, 370 (1987).
[34] J. M. Leinaas, arXiv:0911.1111.
[35] J. M. Leinaas, M. Horsdal, and T. H. Hansson, Phys. Rev. B **80**, 115327 (2009).
[36] K.-I. Imura, Y. Yoshimura, Y. Takane, and T. Fukui, Phys. Rev. B **86**, 235119 (2012).
[37] V. Parente, P. Lucignano, P. Vitale, A. Tagliacozzo, and F. Guinea, Phys. Rev. B **83**, 075424 (2011).
[38] E. T. Newman and R. Penrose, J. Math. Phys. **7**, 863 (1966).
[39] A. A. Abrikosov, Jr., arXiv:hep-th/0212134.
[40] Reference [26] does not mention boundary conditions and concludes that even in the absence of an external magnetic field, the spherical Dirac operator has zero-energy states, $E = 0$, which does not agree with our results.
[41] A. Lichnerowicz, C. R. Acad. Sci. Paris **257**, 7 (1963).
[42] F. W. J. Olver, A. B. Olde Daalhuis, D. W. Lozier, B. I. Schneider, R. F. Boisvert, C. W. Clark, B. R. Miller, and B. V. Saunders, NIST Digital Library of Mathematical Functions, 2016.
[43] V. Venkatachalam, A. Yacoby, L. Pfeiffer, and K. West, Nature (London) **469**, 185 (2010).
[44] A. Kanda, B. J. Baelus, F. M. Peeters, K. Kadowaki, and Y. Ootuka, Phys. Rev. Lett. **93**, 257002 (2004).
[45] T. Cren, L. Serrier-Garcia, F. Debontridder, and D. Roditchev, Phys. Rev. Lett. **107**, 097202 (2011).